Int. J. Multiphase Flow Vol. 11, No. 4, pp. 459–479, 1985
Printed in the U.S.A.

0301-9322/85 $3.00 + .00

INFLUENCE OF BUBBLE EXPANSION AND RELATIVE VELOCITY ON THE PERFORMANCE AND STABILITY OF AN AIRLIFT PUMP

NICHOLAS APAZIDIS
Department of Mechanics, Royal Institute of Technology, S-100 44 Stockholm, Sweden

(*Received* 27 *November* 1983; *in revised form* 29 *October* 1984)

Abstract—An airlift pump which raises liquid by means of compressed air introduced near the lower end of the eduction pipe is an example of a self-control system. It has been shown by Hjalmars (1973) that an occasionally observed breakdown in the self-control mechanism, which leads to instability, is due to the fact that the control mechanism is delayed, with the effect that a small, time-dependent perturbation of the stationary flow satisfies a differential equation with delayed argument. This investigation was carried out with the assumption of a single-phase flow of an ideal incompressible liquid. The aim of the present study is to consider the stability conditions of an airlift pump within the frame of a more general flow model, namely a separate two-phase flow of compressible gas and incompressible liquid, which takes into account the effects of the expasion of gas bubbles during their lift and of the relative velocity, i.e. the difference in the velocity of gas bubbles and the liquid.

1. INTRODUCTION

An airlift pump is investigated as to its performance and stability within the frame of a separate two-phase flow model of compressible gas and incompressible liquid.

An air compressor is assumed to generate air bubbles of approximately the same radius, much smaller than that of the cross-section of the eduction pipe, and distribute them uniformly across the cross-section, allowing the bubbly flow approximation. Assuming further one-dimensional flow, isothermal expansion of air bubbles, according to Boyle's law and neglecting the wall friction we write down separate continuity and momentum equations for each phase. Combining the later two we eliminate forces due to mutual hydrodynamic drag. Two additional equations are required, however, one being an empirical relation expressing the relative velocity, i.e. difference in the velocities of gas and liquid in terms of bubble dimensions, bubble concentration and liquid properties. The second relation is the equation of state for gas.

Decomposing the variables in the stationary and small time-dependent perturbated quantities we obtain a system of ordinary differential equations of the first order with initial conditions for the stationary parts and a system of partial differential equations of the first order with boundary conditions for the perturbations. Solving the system for the stationary values and satisfying the initial conditions we find values of the rise, i.e. the height of the upper pipe opening over the free water level in the basin as function of air and water fluxes. Solution of the boundary value problem for the perturbations gives values of the critical rise, i.e. values of the rise for which instability sets in, as function of air flux alone.

The problem is treated as a one-dimensional separate two-phase flow of compressible gas and incompressible liquid. The wall friction, temperature effects and the velocity of water outside the close neighbourhood of the lower pipe opening are neglected.

2. FLOW IN THE PIPE [$0 \leq z \leq L$]

The gas and the liquid phases are considered separately, but variations of the variables across the cross-section of the pipe are neglected. Introducing the local volumetric concentration of gas $a(z, t)$ we obtain the following forms of the continuity equations for the liquid (index L), along the vertical z-axis, shown in figure 8

$$(1 - a)_{,t} + [(1 - a)v_L]_{,z} = 0, \qquad [2.1]$$

since ρ_L = const.
and gas (index G)

$$(a\rho_G)_{,t} + (a\rho_G v_G)_{,z} = 0. \tag{2.2}$$

The momentum equations for each phase read (see Wallis (1969))

$$\rho_L v_{L,t} + \rho_L v_L v_{L,z} + \rho_L g - f_L + p_{,z} = 0, \tag{2.3}$$

$$\rho_G v_{G,t} + \rho_G v_G v_{G,z} + \rho_G g - f_G + p_{,z} = 0, \tag{2.4}$$

where f_L and f_G are forces entirely due to mutial hydrodynamic drag. Since action and reaction are equal we have

$$F_L = f_L(1 - a) = -f_G a = -F_G, \tag{2.5}$$

where F_L and F_G are defined as equivalent of the f's per unit volume of the whole flow field. Multiplying [2.3] by $(1 - a)$ and adding [2.4] multiplied by a we obtain after neglection of all terms proportional to $\rho_G(\rho_G \ll \rho_L)$ the following equation:

$$\rho_L(1 - a)v_{L,t} + \rho_L(1 - a)v_L v_{L,z} + (1 - a)\rho_L g + p_{,z} = 0. \tag{2.6}$$

Equations [2.1], [2.2] and [2.6] form a system of three equations with five unknowns: a, v_L, v_G, ρ_G and p, therefore two additional equation's are required. One of which is the equation of state for the gas:

$$p = \text{const} \cdot \rho_G, \tag{2.7}$$

and the other is the equation, defining the relative velocity, i.e. the difference in the velocity of gas bubbles v_G and the liquid v_L, and is an empirical relation of the following form (Wallis 1969):

$$v_G - v_L = (1 - a)^{n-1} v_\infty, \tag{2.8}$$

where n is a function of a suitably defined Reynolds number and v_∞ is the terminal velocity of gas bubbles and is expressed in terms of the fluid properties and bubble size.

The dependence of the terminal rise velocity of a single bubble, v_∞, upon fluid properties has been determined experimentally by Peebles & Garber (1953). For the gas density negligible with respect to liquid density the relations are shown in table 1, and plotted in figure 1.

3. FLOW IN THE AIR INJECTION ZONE $[-\delta, 0]$

The equation of continuity is identical with [2.1],

$$(1 - a)_{,t} + [(1 - a)v_L]_{,z} = 0. \tag{3.1}$$

The momentum equation for the mixture with an introduction of the pressure drop term due to friction losses of the sudden expansion, contraction and form type losses in this zone, reads:

$$\rho_L(1 - a)v_{L,t} + \rho_L(1 - a)v_L v_{L,z} + (1 - a)\rho_L g + p_{,z} + p_{f,z} = 0. \tag{3.2}$$

Table 1. Terminal velocity of single gas bubbles in liquids (Peebles & Garber 1953)

Region	Terminal velocity	n	Range of applicability
1	$v_\infty = \frac{2r^2 g}{9\nu_L}$	2	$r \leq 7 \cdot 10^{-5}$ m
2	$v_\infty = 0.33\, g^{3/4} \nu_L^{-1/2} r^{5/4}$	$\frac{7}{4}$	$7 \cdot 10^{-5}$ m $< r \leq 1 \cdot 10^{-3}$ m
3	$v_\infty = 1.35 \left(\frac{\sigma}{\rho_L r}\right)^{1/2}$	$\frac{3}{2}$	$1 \cdot 10^{-3}$ m $< r \leq 2 \cdot 10^{-3}$ m
4	$v_\infty = 1.53 \left(\frac{g\sigma}{\rho_L}\right)^{1/4}$	$\frac{3}{2}$	$2 \cdot 10^{-3}$ m $< r \leq 6.2 \cdot 10^{-3}$ m
5	$v_\infty = (gr)^{1/2}$	0	$6.2 \cdot 10^{-3}$ m $< r$

The pressure drop term $p_{f,z}$ is assumed to stem from form type losses and does not include pressure drop due to the wall friction. In fact, for the pipe dimensions and phase velocities considered in this paper these losses are estimated to account for 5% or less of the form type losses. We assume that

$$p_f \Big|_{-\delta}^{0} = K\rho_L \frac{v_L^2(0, t)}{2}. \qquad [3.3]$$

The value of the loss coefficient K is chosen so, that the theoretical performance points calculated for the model airlift pump described in section 7 fit the experimental data at maximum air and water flow rates, giving the value $K = 4$.

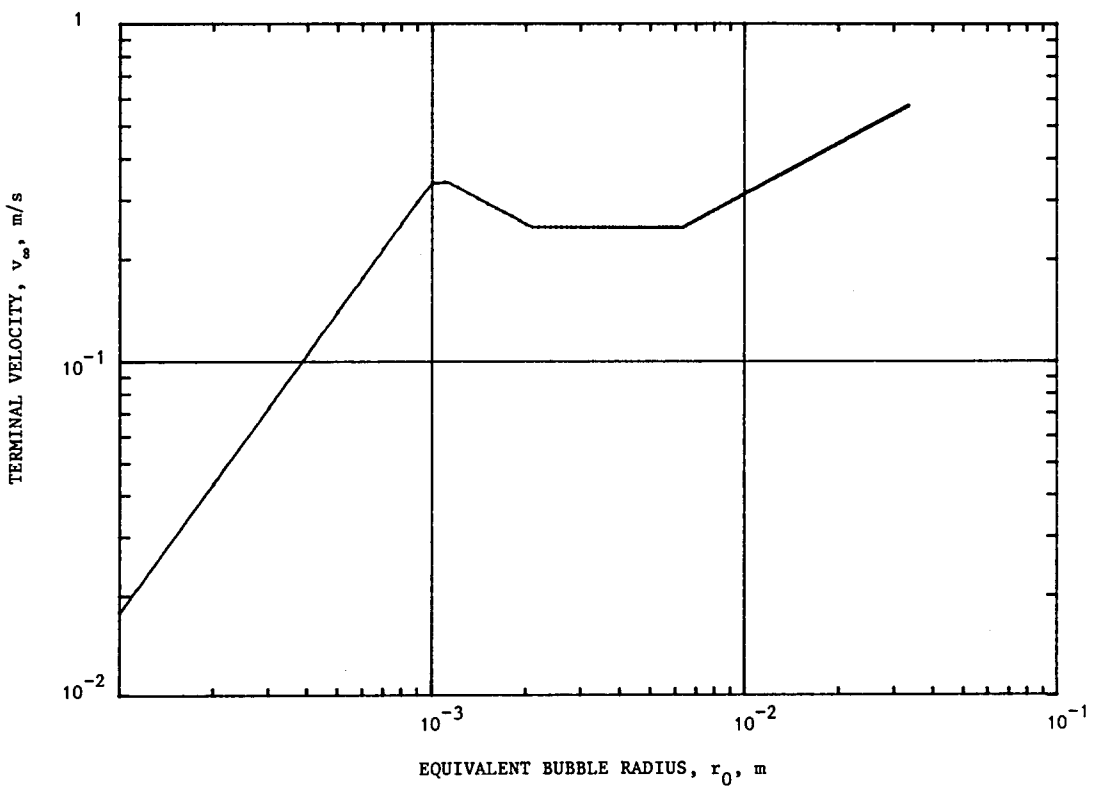

Figure 1. Terminal velocity of air bubbles as function of bubble size, according to Peebles & Garber (1953).

Integrating partially the second term in [3.2] and using [3.1] we obtain:

$$\rho_L \int_{-\delta}^{0} (1-a) v_{L,t}\, dz + \rho_L (1-a) v_L^2 \Big|_{-\delta}^{0} + \rho_L \int_{-\delta}^{0} v_L (1-a)_{,t}\, dz + \rho_L g \int_{-\delta}^{0} (1-a)\, dz + p(0,t) - p(-\delta,t) + K\rho_L \frac{v_L^2(0,t)}{2}. \quad [3.4]$$

Assuming that the length of the zone is small, that is, $\delta \ll v^2/g$ the last equation reduces to:

$$p(0,t) = p(-\delta,t) - \rho_L [1-a(z,t)] v_L^2(z,t) \Big|_{-\delta}^{0} - K\rho_L \frac{v_L^2(0,t)}{2}. \quad [3.5]$$

Equation [3.1] gives in the same way

$$[1-a(z,t)] v_L(z,t) = [1-a(-\delta,t)] v_L(-\delta,t), \quad [3.6]$$

which together with [3.5] and since a $(-\delta, t) = 0$ results in

$$p(z,t) = p(-\delta,t) - \rho_L Q^2(t) \frac{a(z,t)}{1-a(z,t)} - K\rho_L \frac{Q^2(t)}{2[1-a(z,t)]}, \quad [3.7]$$

where $Q(t) = v_L(-\delta, t)$.

We are now going to derive an equation defining the void fraction in terms of gas and liquid volume flows and the relative velocity. Suppose that in the slice between z and $z + dz$ it is injected per second and unit section area the quantity of air which under atmospheric pressure p_a would have had the volume:

$$dV = \vartheta(z)\, dz. \quad [3.8]$$

Consider the gas volume injected in the slice between z and $z + dz$ per unit time, compressed to pressure p

$$\frac{dV}{dt} = \pi R^2 \frac{p_a}{p} \vartheta\, dz, \quad [3.9]$$

where R is the radius of the cross-section of the pipe. If dz is the distance covered by the air bubble during time dt then

$$dt = \frac{dz}{v_L + v_\infty (1-a)^{n-1}}. \quad [3.10]$$

We thus obtain:

$$da = \frac{dV}{\pi R^2 dz} = \frac{p_a}{p(z,t)} \frac{\vartheta\, dz}{v_L(z,t) + v_\infty [1-a(z,t)]^{n-1}}, \quad [3.11]$$

or

$$p(z,t) \left(\frac{Q(t)}{1-a(z,t)} + v_\infty (1-a(z,t))^{n-1} \right) da = p_a \vartheta\, dz. \quad [3.12]$$

Introducing $p(z, t)$ according to [3.7], integrating the obtained relation from $-\delta$ to 0 and neglecting the terms proportional to $\rho_L Q^2$, which are small as compared to $p(-\delta, t)$ we obtain an approximate equation, defining the void fraction $a(0, t)$ at the end of the air injection zone. For $n \neq 0$ this equation reads:

$$ln[1 - a(0, t)] - \frac{v_\infty(0, t)}{nQ(t)} [1 - (1 - a(0, t))^n] = - \frac{p_a}{p(-\delta, t)} \frac{q}{Q(t)} \qquad [3.13]$$

and for region 5 ($n = 0$):

$$a(0, t) = 1 - \exp\left\{ - \left[\frac{p_a}{p(-\delta, t)} \frac{q}{Q(t) + v_\infty(0, t)} \right] \right\}, \qquad [3.14]$$

where

$$q = \int_{-\delta}^{0} \vartheta \, dz$$

is the total volume of air injected per unit time and unit section area at atmospheric pressure.

4. FLOW IN THE BASIN

Following the presentation by Hjalmars (1973) we assume an irrotational potential flow in this region. Introduction of the velocity potential in the continuity equation gives the Laplace equation. Integrating the momentum equation written in terms of the velocity potential from the lowest point of the air-injection zone $z = -\delta$ to the free water level $z = L - H$, see figure 8, the following relation is obtained:

$$p(-\delta, t) = p_a + \rho_L g(L - H) - \tfrac{1}{2} \rho_L Q^2(t) + \rho_L \dot{\phi}(-\delta, t), \qquad [4.1]$$

where $\phi(z, t)$ is the velocity potential.

Since $\phi(z, t)$ satisfies the Laplace equation and the boundary conditions

$$-\phi_z = Q(t) \text{ for } z = -\delta \quad \text{and} \quad \phi = 0 \text{ for } z = L - H, \qquad [4.2]$$

the ϕ-fields for different t-values are all similar and proportional to $Q(t)$. We have thus:

$$\phi(-\delta, t) = -lQ(t), \qquad [4.3]$$

where l is a length, which can be calculated from the stationary flow in the basin, and which is of the same order of magnitude as the distance from the air-injection zone to the nearest point in the basin, where the water velocity is negligible. Since we assume the water velocity in the basin is small already on small distances from the lower pipe opening, we neglect the $\dot{\phi}$ term in [4.1]. This is equivalent to the assumption that the flow in the basin is quasi-stationary, so that the local time derivatives of the velocity may be neglected.

5. THE STATIONARY STATE

Consider small time-dependent perturbations of the stationary values $\hat{a}(z)$, $\hat{v}_L(z)$, $\hat{v}_G(z)$, $\hat{p}(z)$ and $\hat{Q}$.

$$a(z, t) = \hat{a}(z)[1 + \epsilon\alpha(z, t)], \tag{5.1}$$

$$v_L(z, t) = \hat{v}_L(z)[1 + \epsilon u_L(z, t)], \tag{5.2}$$

$$v_G(z, t) = \hat{v}_G(z)[1 + \epsilon u_G(z, t)], \tag{5.3}$$

$$p(z, t) = \hat{p}(z) + \epsilon\pi(z, t), \tag{5.4}$$

$$Q(t) = \hat{Q}[1 + \epsilon\eta(t)]. \tag{5.5}$$

Introducing relations [5.1]–[5.5] in [2.1], [2.2], [2.6] and using [2.8] we obtain various systems of ordinary differential equations for the stationary values of the gas volumetric concentration $\hat{a}(z)$ and pressure $\hat{p}(z)$ for various regions, depending on the bubble dimensions. In region $3(10^{-3}\ m < r \leq 2 \cdot 10^{-3}\ m)$, for example, the system of two equations with initial conditions takes the following form:

$$\begin{cases} \hat{a}' = \rho_L g(1 - \hat{a}) \left\{ \left[\dfrac{k}{\hat{a}^2} + \dfrac{b}{(1 - \hat{a})^2}\hat{p} - \dfrac{1}{2}c(1 - \hat{a})^{-1/2}\hat{p}^{7/6} \right] \right. \\ \qquad \left. \cdot \left[\dfrac{b}{1 - \hat{a}} + \dfrac{7}{6}c(1 - \hat{a})^{1/2}\hat{p}^{1/6} \right]^{-1} - \rho_L \dfrac{b^2}{(1 - \hat{a})^2} \right\}^{-1} \qquad [5.6] \\ \hat{p}' = -\rho_L g(1 - \hat{a}) - \rho_L \dfrac{b^2}{(1 - \hat{a})^2}\hat{a}', \qquad [5.7] \end{cases}$$

satisfying the initial conditions that the values of $\hat{a}(0)$, $\hat{p}(0)$ are those, evaluated by means of [4.1], [3.12] and [3.4]. Here we have introduced:

$$b = [1 - \hat{a}(0)]\hat{v}_L(0), \quad k = \hat{a}(0)\hat{p}(0)\hat{v}_G(0) \quad \text{and} \quad c = \hat{v}_\infty(0)\hat{p}^{-1/6}(0)$$

with $\hat{v}_\infty(0)$ according to table 1.

The value of the rise H is chosen so that $\hat{p}(L) = p_a$. Analogical systems of equations with initial conditions are obtained for other regions. Solution of these equations gives values of:

$$\text{the dimensionless rise } \Delta = \frac{H}{L}, \tag{5.8}$$

versus,

$$\text{the dimensionless water flux } \hat{\Gamma} = \hat{Q}(2gL)^{-1/2} \tag{5.9}$$

for various values of

$$\text{the dimensionless air flux } \gamma = q(2gL)^{-1/2} \tag{5.10}$$

and different bubble sizes and pipe lengths, see figures 2, 3 and 4.

6. PERTURBATIONS OF THE STATIONARY STATE

Equations of continuity and momentum in the pipe, air injection zone and the basin give the following system of linear partial differential equations of the first order with the

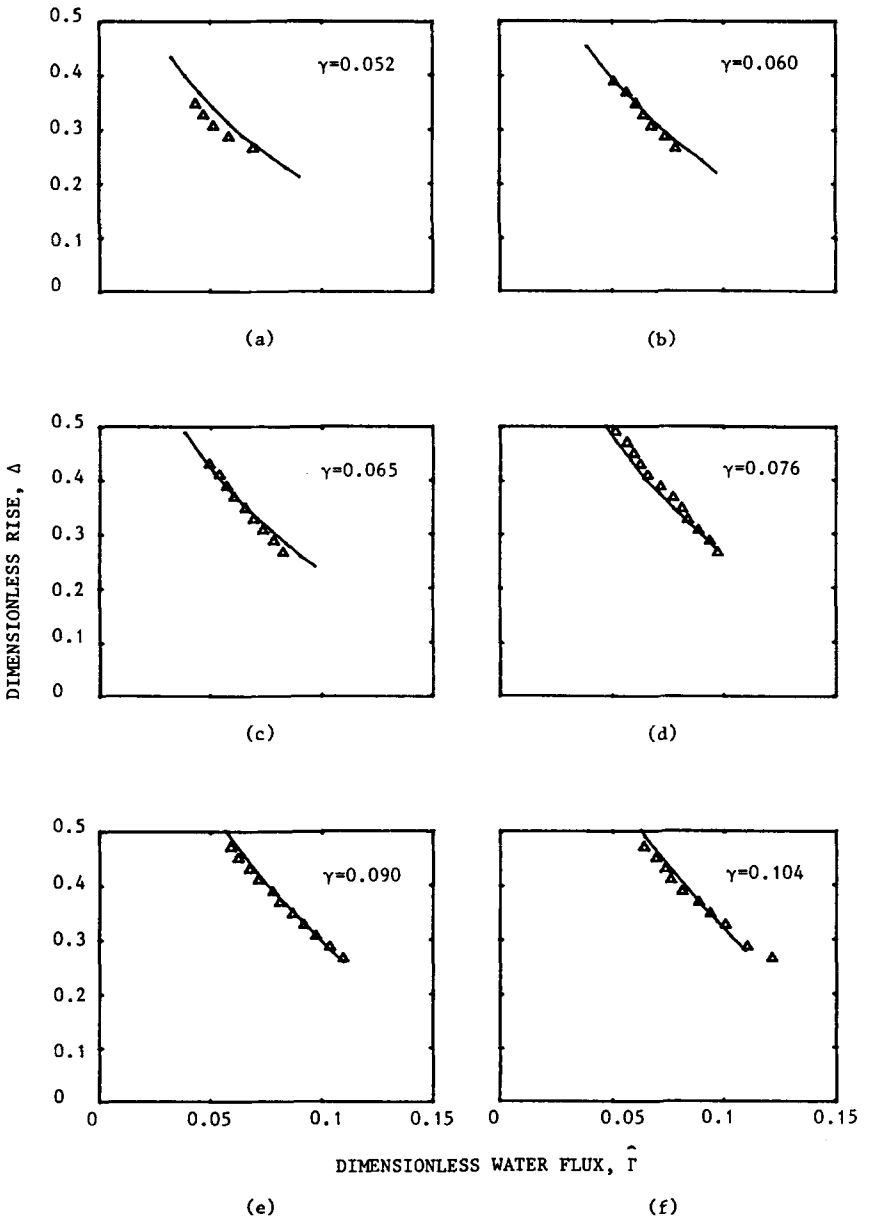

Figure 2. Comparison of theoretical performance with experimental values for a model airlift pump. $L = 0.49$ m, $r_0 = 1 \cdot 10^{-3}$ m.

boundary conditions for the perturbations $\alpha(z, t)$, $u_L(z, t)$ and $\pi(z, t)$:

$$\begin{aligned}&\hat{a}\hat{p}\alpha_{,t} + \hat{a}\pi_{,t} + (\hat{a}\hat{p}\hat{v}_L)'(\alpha + u_L) + (\hat{a}\hat{v}_L)'\pi + \hat{a}\hat{p}\hat{v}_L(\alpha_{,z} + u_{L,z})\\ &+ \hat{a}\hat{v}_L\pi_{,z} + c_n(0)\left(1 - \frac{m}{3}\right)[\hat{a}(1-\hat{a})^{n-1}\hat{p}^{-m/3}]'\pi\\ &+ c_n(0)\left(1 - \frac{m}{3}\right)\hat{a}(1-\hat{a})^{n-1}\hat{p}^{-m/3}\pi_{,z} + c_n(0)[\hat{a}(1-\hat{a})^{n-2}\\ &\cdot(1 - n\hat{a})\hat{p}^{1-m/3}]'\alpha + c_n(0)\hat{a}(1-\hat{a})^{n-2}(1 - \hat{n}\hat{a})\hat{p}^{1-m/3}\alpha_{,z} = 0,\end{aligned} \tag{6.1}$$

$$\hat{a}\alpha_{,t} + (\hat{a}\hat{v}_L)'\alpha + \hat{a}\hat{v}_L\alpha_{,z} - \hat{Q}u_{L,z} = 0, \tag{6.2}$$

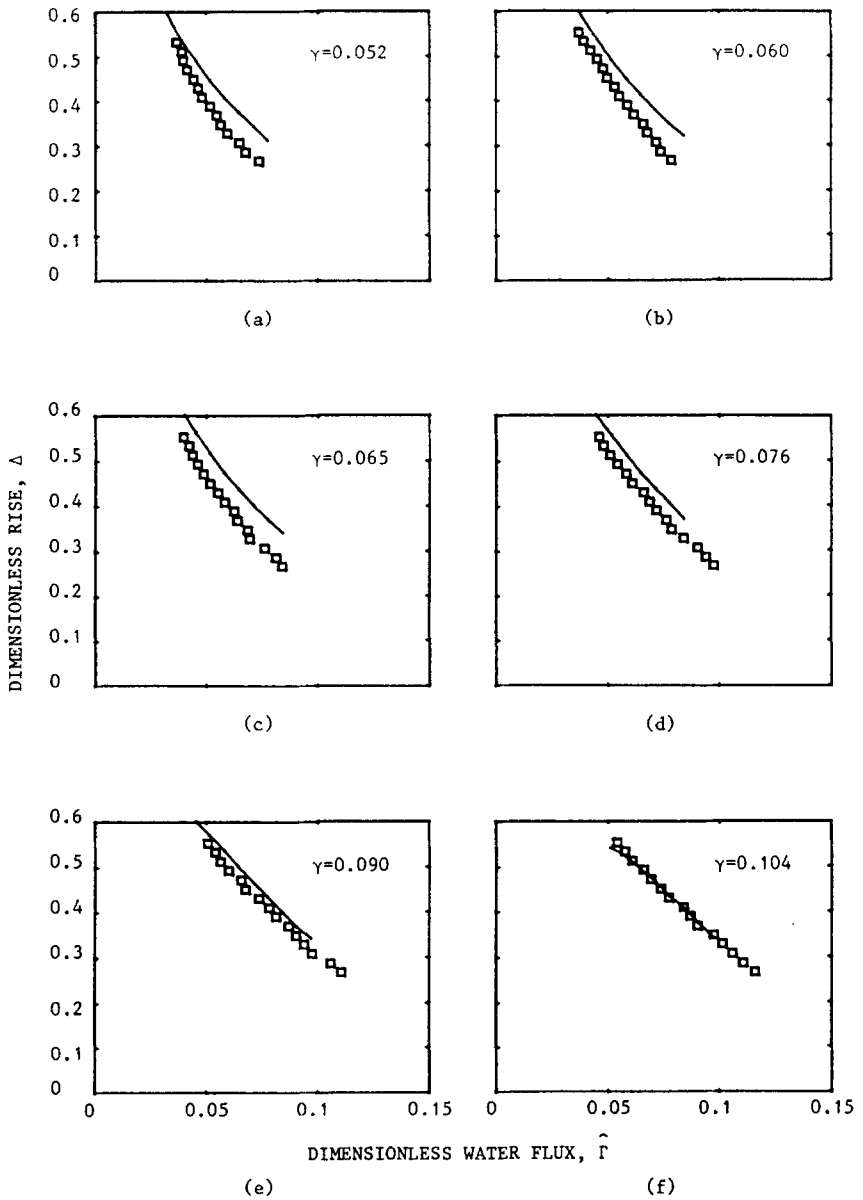

Figure 3. Comparison of theoretical performance with experimental values for a model airlift pump. $L = 0.49$ m, $r_0 = 5 \cdot 10^{-4}$ m.

$$\rho_L \hat{Q} u_{L,t} + 2\rho_L \hat{Q} \hat{v}_L' u_L + \rho_L \hat{Q} \hat{v}_L u_{L,z} + \frac{\hat{a}}{1 - \hat{a}} \hat{p}' \alpha + \pi_{,z} = 0. \qquad [6.3]$$

Boundary conditions

$$\hat{Q} u_L(0, t) - \hat{a}(0) \hat{v}_L(0) \alpha(0, t) = \hat{Q} \eta(t), \qquad [6.4]$$

$$\pi(0, t) = -\rho_L \hat{Q}^2 \left(\frac{1 + \hat{a}(0)}{1 - \hat{a}(0)} \eta(t) + \frac{\hat{a}(0)}{[1 - \hat{a}(0)]^2} \alpha(0, t) + \frac{K}{[1 - \hat{a}(0)]^2} \eta(t) + K \frac{\hat{a}(0)}{[1 - \hat{a}(0)]^3} \alpha(0, t) \right), \qquad [6.5]$$

$$- \frac{\hat{a}(0)}{1 - \hat{a}(0)} \alpha(0, t) - \frac{\hat{v}_\infty(0)}{n \hat{Q}} \hat{a}(0) [1 - \hat{a}(0)]^{n-1} \alpha(0, t)$$

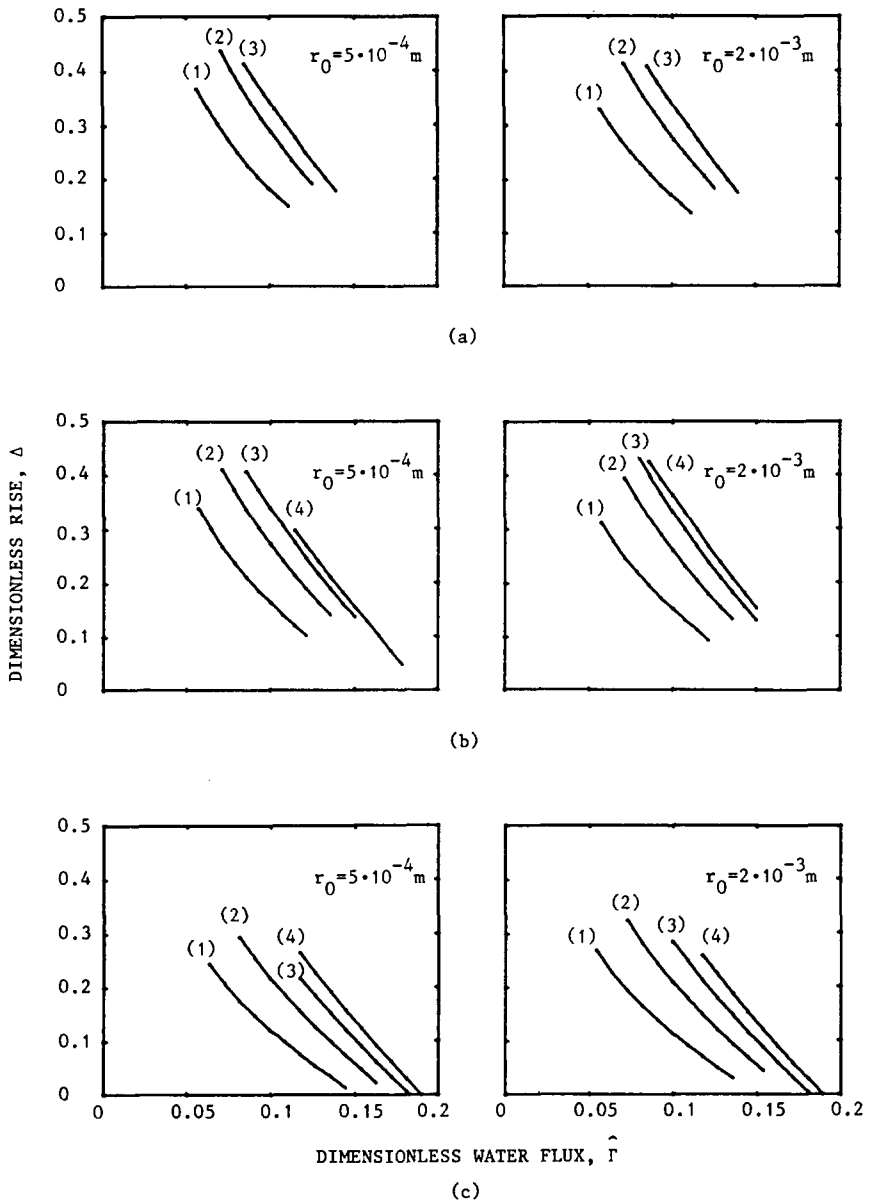

Figure 4. Theoretical performance of airlift pumps with various pipe lengths. (a) L = 5 m; (b) L = 10 m; (c) L = 25 m; (1): γ = 0.04; (2): γ = 0.07; (3): γ = 0.1; (4): γ = 0.13.

$$+\frac{\hat{v}_\infty(0)}{n\hat{Q}}[1-(1-\hat{a}(0))^n]\eta(t)=\frac{p_a}{p(-\delta)}\frac{q}{\hat{Q}}\eta(t). \qquad [6.6]$$

In region 5 (6.6) takes the form:

$$\alpha(0,t)=-\frac{1}{\hat{a}(0)}\frac{p_a}{\hat{p}(-\delta)}\frac{q\hat{Q}}{[\hat{Q}+\hat{v}_\infty(0)]^2}\exp\left\{-\left[\frac{p_a}{\hat{p}(-\delta)}\frac{q}{\hat{Q}+\hat{v}_\infty(0)}\right]\right\}\eta(t), \qquad [6.6a]$$

$$\pi(L,t)=0, \qquad [6.7]$$

where $c_n(0)=\hat{v}_\infty(0)\hat{p}^{m/3}(0)$ and m depends on the region and is equal to the exponent of r in the table 1.

Assuming that the perturbation of the water velocity at $z = -\delta$, $\eta(t)$ has the form:

$$\eta(t) = \mathrm{Re}[ce^{\omega t}], \tag{6.8}$$

where $c = c_1 + ic_2$ and $\omega = x + iy$ are complex constants, we find the corresponding solution of the system [6.1]–[6.3] with boundary conditions [7.4]–[7.6] in the form

$$\alpha(z, t) = \mathrm{Re}[A(z)e^{\omega t}], \tag{6.9}$$

$$u_L(z, t) = \mathrm{Re}[U(z)e^{\omega t}], \tag{6.10}$$

$$\pi(z, t) = \mathrm{Re}[\Pi(z)e^{\omega t}], \tag{6.11}$$

where

$$A(z) = A_1(z) + iA_2(z), \tag{6.12}$$

$$U(z) = U_1(z) + iU_2(z), \tag{6.13}$$

$$\Pi(z) = \Pi_1(z) + i\Pi_2(z), \tag{6.14}$$

Consider now the same boundary value problem [6.1]–[6.7] for the corresponding complex valued functions

$$\eta^*(t) = ce^{\omega t}, \tag{6.15}$$

$$\alpha^*(z, t) = A(z)e^{\omega t}, \tag{6.16}$$

$$u^*(z, t) = U(z)e^{\omega t}, \tag{6.17}$$

$$\Pi^*(z, t) = \Pi(z)e^{\omega t}. \tag{6.18}$$

Introducing [6.15]–[6.18] into [6.1]–[6.7] and separating real and imaginary parts we obtain a system of 6 ordinary differential equations with initial conditions.

$$A_1' = f_1^{-1}[f_2A_1 + f_3A_2 + f_4U_1 + f_5U_2 + f_6\Pi_1 - y\hat{a}\Pi_2], \tag{6.19}$$

$$U_1' = \hat{Q}^{-1}[x\hat{a} + (\hat{a}\hat{v}_L)']A_1 - y\hat{a}\hat{Q}^{-1}A_2 + \hat{a}\hat{v}_L\hat{Q}^{-1}A_1', \tag{6.20}$$

$$\begin{aligned}\Pi_1' = &-\left\{\frac{\hat{a}}{1-\hat{a}}\hat{p}' + \rho_L\hat{v}_L[x\hat{a} + (\hat{a}\hat{v}_L)']\right\}A_1 + y\rho_L\hat{a}\hat{v}_LA_2 \\ &- [x\rho_L\hat{Q} + 2\rho_L\hat{Q}\hat{v}_L']U_1 + y\rho_L\hat{Q}U_2 - \rho_L\hat{a}\hat{v}_L^2A_1',\end{aligned} \tag{6.21}$$

$$A_2' = f_1^{-1}[-f_3A_1 + f_2A_2 - f_5U_1 + f_4U_2 + y\hat{a}\Pi_1 + f_6\Pi_2] \tag{6.22}$$

$$U_2' = y\hat{Q}^{-1}\hat{a}A_1 + \hat{Q}^{-1}[x\hat{a} + (\hat{a}\hat{v}_L)']A_2 + \hat{Q}^{-1}\hat{a}\hat{v}_LA_2', \tag{6.23}$$

$$\begin{aligned}\Pi_2' = &-y\rho_L\hat{a}\hat{v}_LA_1 - \left\{\frac{\hat{a}}{1-\hat{a}}\hat{p}' + \rho_L\hat{v}_L[x\hat{a} + (\hat{a}\hat{v}_L)']\right\}A_2 \\ &-y\rho_L\hat{Q}U_1 - [x\rho_L\hat{Q} + 2\rho_L\hat{Q}\hat{v}_L']U_2 - \rho_L\hat{a}\hat{v}_L^2A_2'.\end{aligned} \tag{6.24}$$

where

$$f_1(z) = \rho_L \hat{a}\hat{v}_L^2 g_1 - \hat{p}\hat{a}^2\hat{v}_L^2\hat{Q}^{-1} - \hat{a}\hat{p}\hat{v}_L - g_2 \qquad [6.25]$$

$$f_2(z) = x\hat{a}\hat{p} + (\hat{a}\hat{p}\hat{v}_L)' + g_2' + \hat{a}\hat{p}\hat{v}_L\hat{Q}^{-1}[x\hat{a} + (\hat{a}\hat{v}_L)'] - g_1\left\{\frac{\hat{a}}{1-\hat{a}}\hat{p}' + \rho_L\hat{v}_L[x\hat{a} + (\hat{a}\hat{v}_L)']\right\}, \qquad [6.26]$$

$$f_3(z) = -y\hat{a}\hat{p} - y\hat{a}^2\hat{p}\hat{v}_L\hat{Q}^{-1} + y\rho_L\hat{a}\hat{v}_L g_1, \qquad [6.27]$$

$$f_4(z) = (\hat{a}\hat{p}\hat{v}_L)' - g_1(x\rho_L\hat{Q} + 2\rho_L\hat{Q}\hat{v}_L), \qquad [6.28]$$

$$f_5(z) = y\rho_L\hat{Q}g_1, \qquad [6.29]$$

$$f_6(z) = x\hat{a} + g_1', \qquad [6.30]$$

$$g_1(z) = \hat{a}\hat{v}_L + c_n(0)\left(1 - \frac{m}{3}\right)\hat{a}(1-\hat{a})^{n-1}\hat{p}^{-m/3}, \qquad [6.31]$$

$$g_2(z) = c_n(0)\hat{a}(1-\hat{a})^{n-2}(1 - n\hat{a})\hat{p}^{1-m/3}. \qquad [6.32]$$

Initial conditions

$$A_1(0) = \frac{\frac{v_\infty(0)}{n\hat{Q}}[1 - (1-\hat{a}(0))^n] - \frac{p_a}{\hat{p}(-\delta)}\frac{q}{\hat{Q}}}{\frac{v_\infty(0)}{\hat{Q}}\hat{a}(0)(1-\hat{a}(0))^{n-1} + \frac{\hat{a}(0)}{1-\hat{a}(0)}}c_1 = \alpha_0 c_1, \qquad [6.33]$$

$$U_1(0) = \left[1 + \hat{a}(0)\frac{\hat{v}_L(0)}{\hat{Q}}\alpha_0\right]c_1, \qquad [6.34]$$

$$\Pi_1(0) = \frac{-\rho_L\hat{Q}^2\left[\frac{1+\hat{a}(0)}{1-\hat{a}(0)} + \frac{\hat{a}(0)}{[1-\hat{a}(0)]^2}\alpha_0 + \frac{K}{[1-\hat{a}(0)]^2} + K\frac{\hat{a}(0)}{[1-\hat{a}(0)]^3}\alpha_0\right]c_1}{\eta(t)}, \qquad [6.35]$$

and identical relations for $A_2(0)$, $U_2(0)$, $\Pi_2(0)$ and c_2.

In region 5 the form of α_0 is different and is obtained by means of [6.6a]:

$$\alpha_0 = -\frac{1}{\hat{a}(0)}\frac{p_a}{\hat{p}(-\delta)}\frac{q\hat{Q}}{[\hat{Q} + \hat{v}_\infty(0)]^2}\exp\left\{-\left[\frac{p_a}{\hat{p}(-\delta)}\frac{q}{\hat{Q} + \hat{v}_\infty(0)}\right]\right\}. \qquad [6.36]$$

Additional condition (6.7) gives:

$$\Pi_1(L) = 0, \qquad [6.37]$$

$$\Pi_2(L) = 0. \qquad [6.38]$$

Considering the neutral stability mode, $x = 0$ and solving system [6.19]–[6.24] with initial conditions [6.33]–[6.35] we are seeking values of the water velocity $\hat{Q}$ and frequency

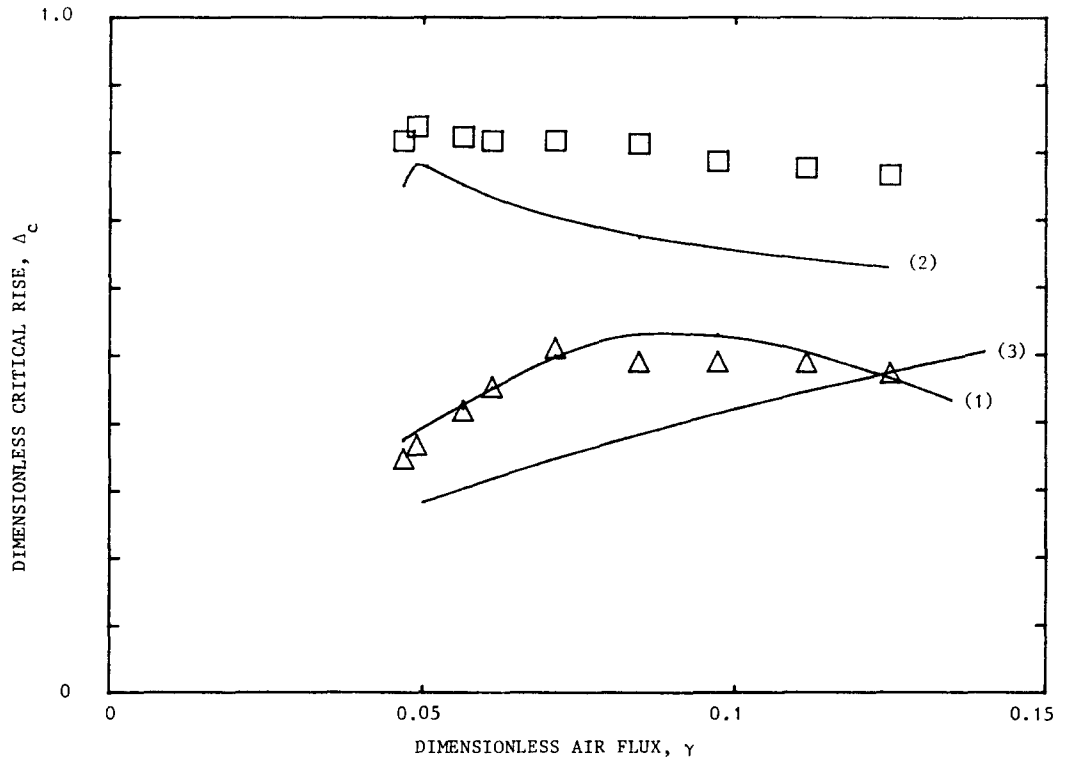

Figure 5. Comparison of neutral stability curves with experimental values for a model airlift pump. Theoretical curves: (1): $r_0 = 1 \cdot 10^{-3}$ m; (2): $r_0 = 5 \cdot 10^{-4}$ m; (3): single-phase theory. Experimental values: Δ: $r_0 = 1 \cdot 10^{-3}$ m; □: $r_0 = 5 \cdot 10^{-4}$ m.

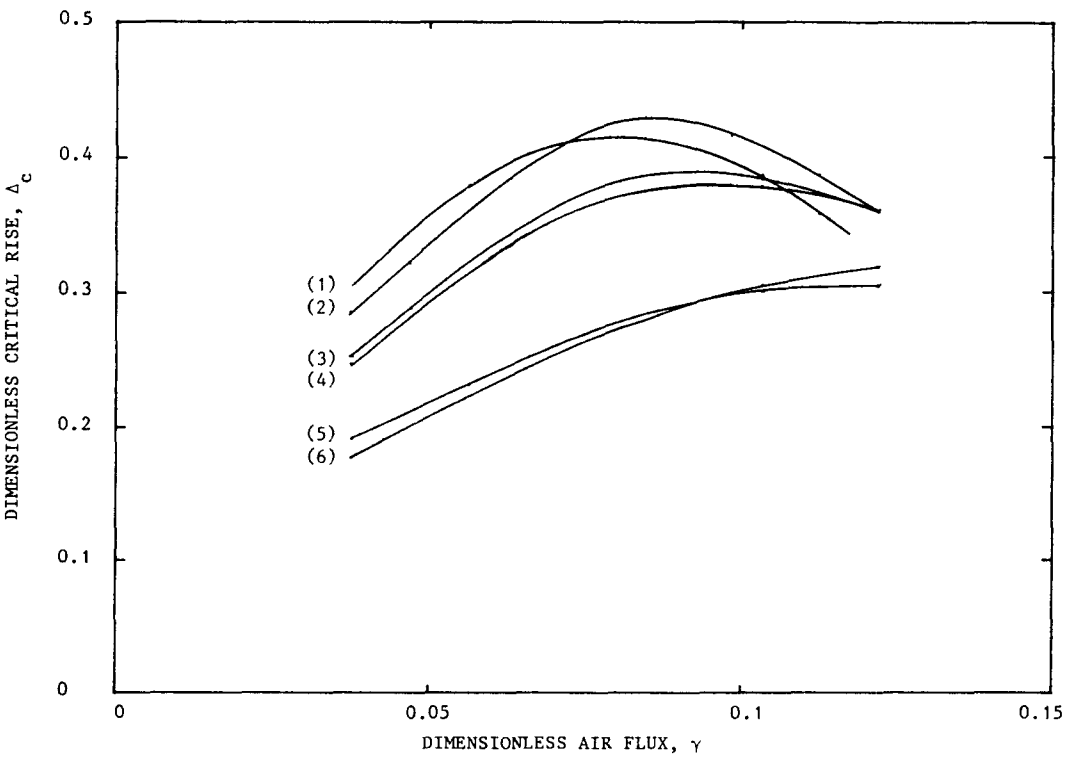

Figure 6. Theoretical neutral stability curves for airlift pumps with various pipe lengths. (1): $L = 5$ m, $r_0 = 5 \cdot 10^{-4}$ m; (2): $L = 5$ m, $r_0 = 2 \cdot 10^{-3}$ m; (3): $L = 10$ m, $r_0 = 5 \cdot 10^{-4}$ m; (4): $L = 10$ m, $r_0 = 2 \cdot 10^{-3}$ m; (5): $L = 25$ m, $r_0 = 5 \cdot 10^{-4}$ m; (6): $L = 25$ m, $r_0 = 2 \cdot 10^{-3}$ m.

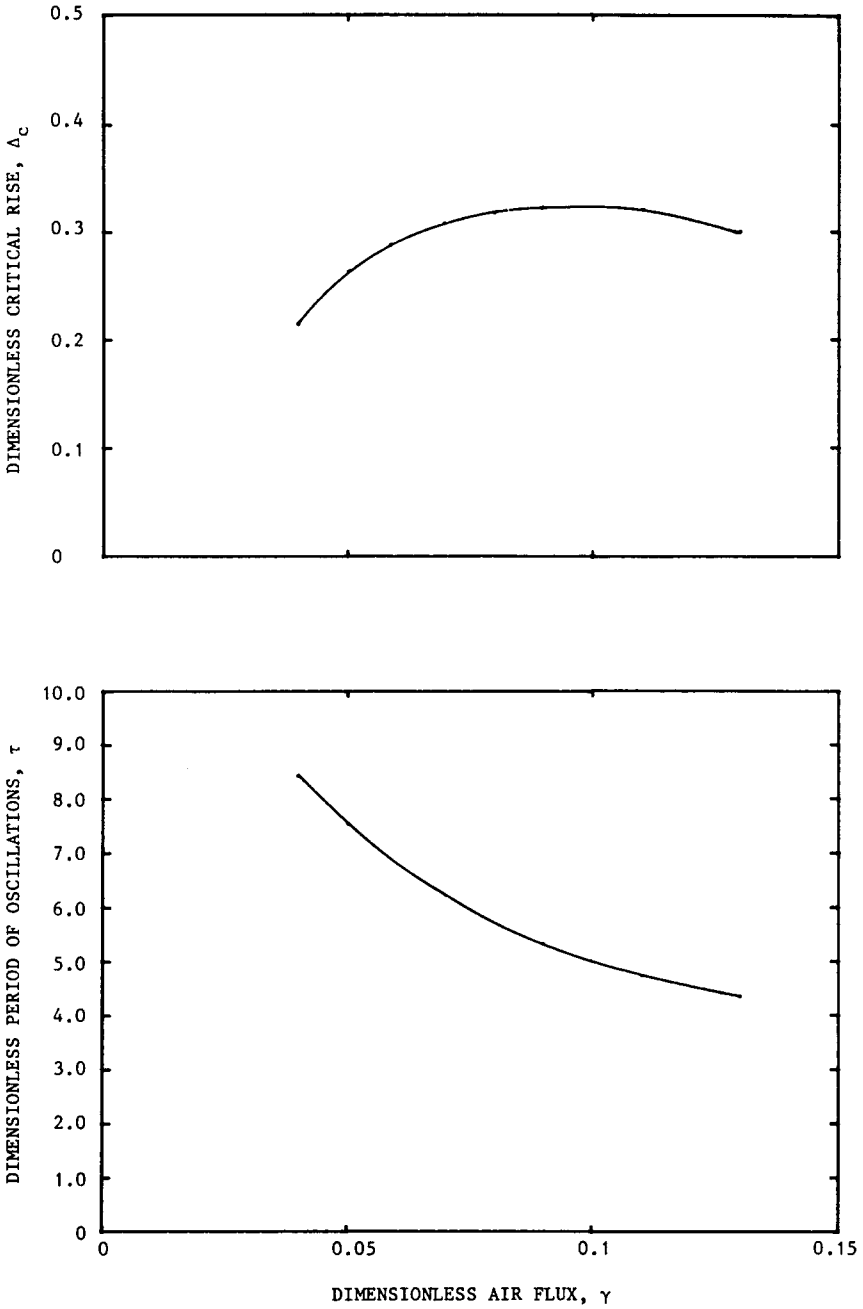

Figure 7. Theoretical neutral stability and oscillation period curves for $L = 25$ m and $K = 8$.

of oscillations y so, that the boundary conditions at the upper end of the pipe [6.37], [6.38] are satisfied. Values of the dimensionless critical rise Δ_c corresponding to these values of $\hat{Q}$ are plotted versus dimensionless air flux γ. These neutral stability curves for the flows with different bubble sizes and for the pumps with various pipe lengths are displayed in figures 5, 6 and 7.

7. EXPERIMENTS AND COMPARISON TO THEORY

A series of simple experiments had been carried out on a model airlift pump illustrated in figure 8. The pump consisted of an air injection chamber and the riser pipe with an elbow at the top. The height of the riser pipe from the end of the air injection chamber to the top (defined as L in figure 8) was 490 mm and the inner diameter 13 mm. The pump was

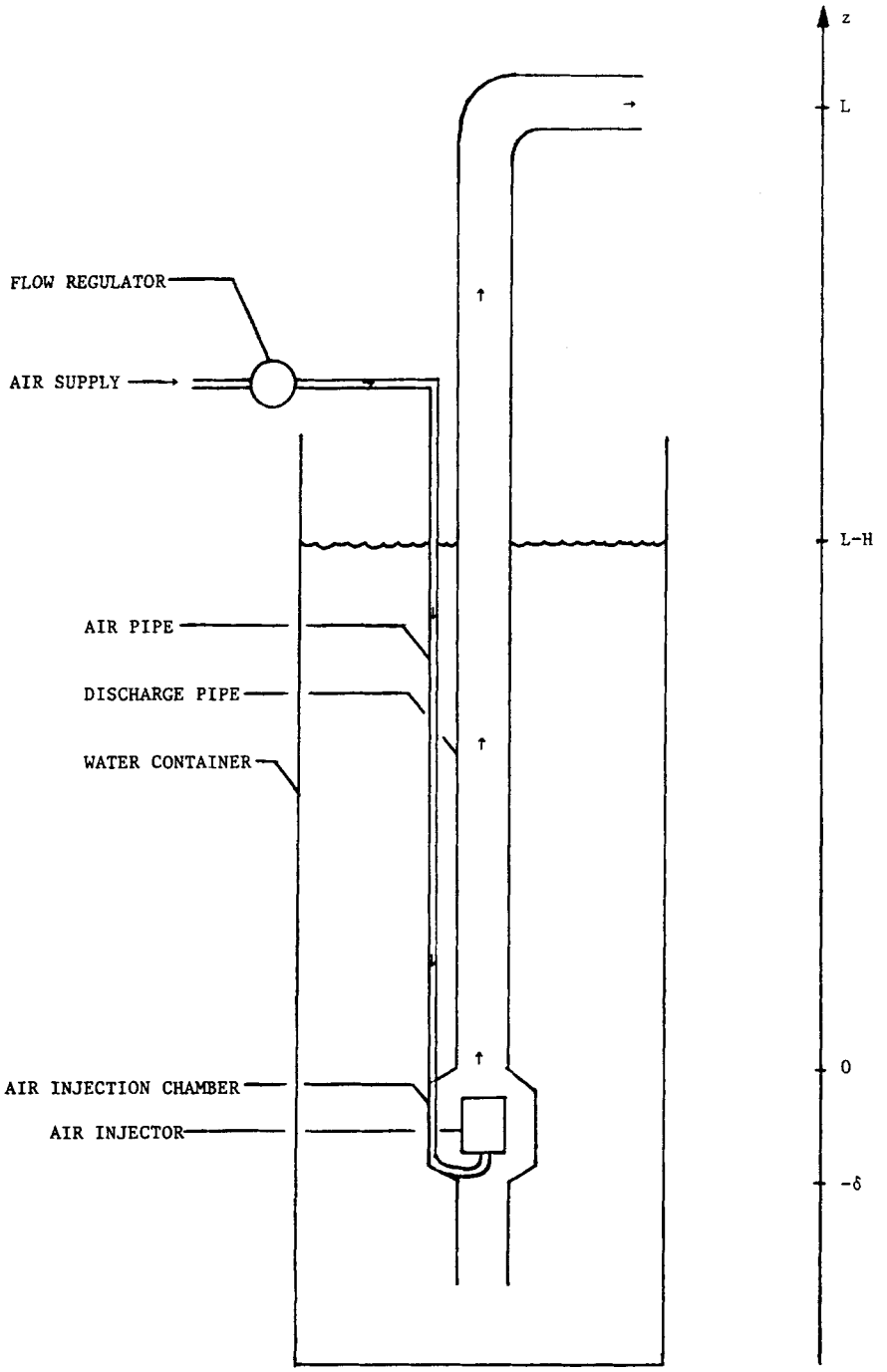

Figure 8. Arrangement of a model airlift pump.

submerged in the water container so that the rise, height of the upper pipe opening over the free water level in the container, (defined as H in figure 8) could be varied from 130 mm to 490 mm.

The air was introduced in the air injection chamber near the lower pipe opening through a porous 15 mm high cylinder. The air flow rate could be varied from 1.23 lit/min to 3.77 lit/min in small steps. For each value of the air flow rate a series of measurements of the corresponding water flow rates at different values of the rise had been carried out. Accuracy of the air and water flow measurements is estimated as approximately ±3% for each quantity. For each value of the air flow rate values of the rise were increased gradually from

130 mm until a critical value was reached and the flow became unstable, resulting in a periodic emptying and refilling of the riser. The critical values of the rise were measured along with the periods of oscillations at each value of the air flow rate.

Dimension of air bubbles generated in the air injection chamber was estimated visually and by measuring the rise velocity of single bubbles in the water container. The air bubble diameter was estimated to be approximately 2 mm during the first series of measurements. The measurements were repeated using smaller air bubbles with a diameter of approximately 1 mm. The size of air bubbles was reduced by an addition of a few drops of a detergent (liquid soap) to water in the container. A 10 to 40% increase in the values of the rise at the corresponding values of air and water flow rates as compared to the flow with 2

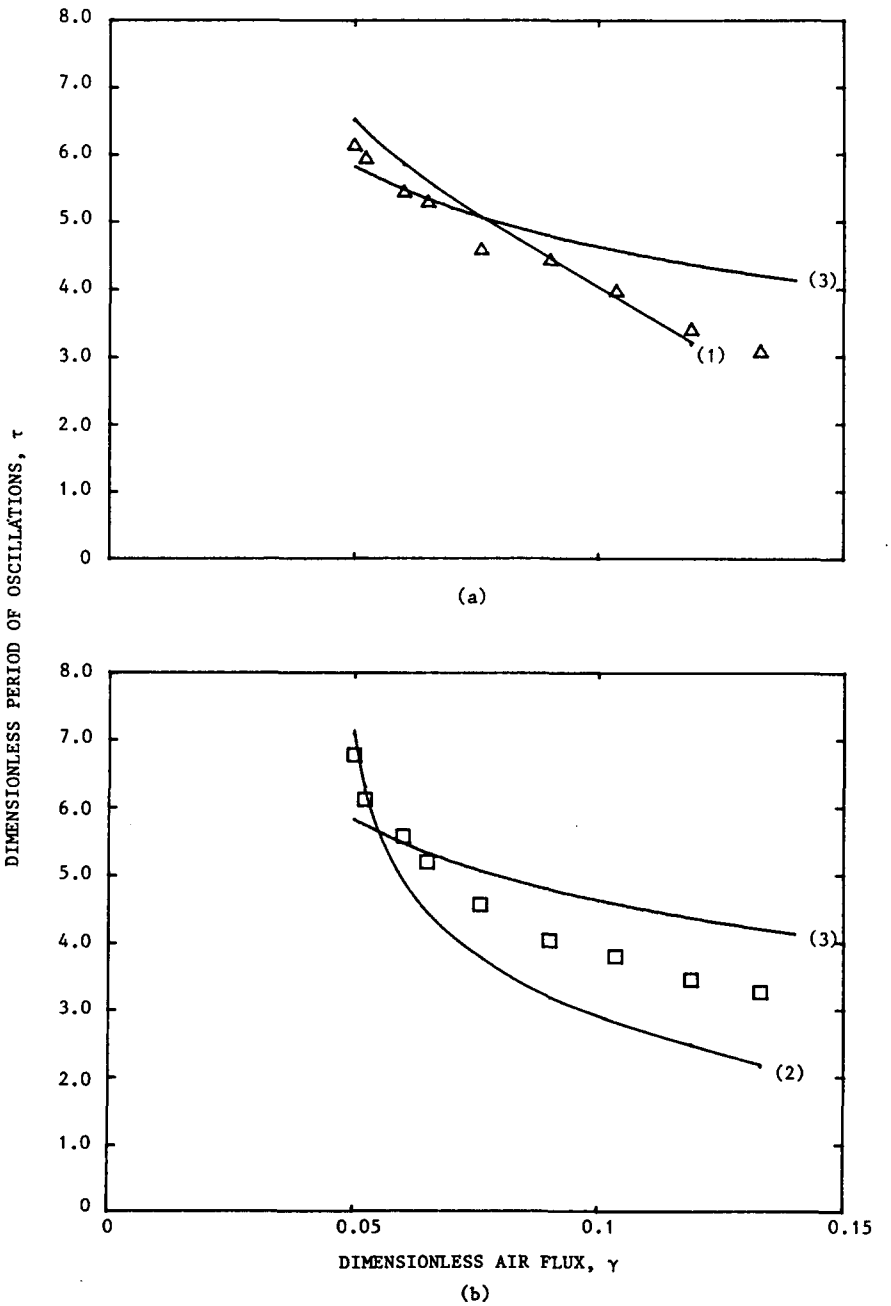

Figure 9. Comparison of oscillation periods with experimental values for a model airlift pump. Theoretical curves: (1): $r_0 = 1 \cdot 10^{-3}$ m; (2): $r_0 = 5 \cdot 10^{-4}$ m; (3): single-phase theory. Experimental values: Δ: $r_0 = 1 \cdot 10^{-3}$ m; □: $r_0 = 5 \cdot 10^{-4}$ m.

mm bubbles had been observed. The increase in the values of the critical rise was even more drastic, especially at the low values of air flow rates, at which the dimensionless critical rise increased from ca 0.35–0.85. At the higher values of air flow rate Δ_c increased from 0.35–0.75.

Period of oscillations decreased from *ca* 2 s–1 s as the air flow rate was increased from minimum to a maximum value. Slightly higher values of the oscillation periods were observed for a flow with smaller bubbles.

The performance and stability data of measurements were recalculated to a dimensionless form and compared to the data obtained by the theoretical analysis. The value of the friction loss coefficient K of the abrupt enlargement, contraction and form losses in the air injection chamber was chosen to fit the value of the rise at the maximum air and water flow rates.

The theoretical performance curves together with the experimental points are plotted in figures 2 and 3. The theoretical curves match the experimental results over the whole range of air and water flow rates within 15% and within 5% at higher values of air flow rates. Reduction of the bubble diameter from 2 mm to 1 mm leads to 30–40% increase in the values of the rise at low values of water flow rates. At higher values of water flow rates the increase is reduced to 5–10%.

Theoretical and experimental values of the critical rise and period of oscillations for the flows with two bubble sizes are shown in figures 5 and 9. For a flow with 2 mm bubbles the critical rise increases from ca 0.35 at $\gamma = 0.045$ to a maximum value of 0.5 at $\gamma = 0.07$. A further increase in the air flow rate leads to a slight decrease in the values of Δ_c which drop from the maximum value to $\Delta_c = 0.48$ at $\gamma = 0.12$. The theoretical curve matches the experimental values fairly well with a maximum deviation of approximately 10%. As a comparison a curve, representing values of the critical rise and obtained by means of single-phase theory in which the friction effects were neglected, see Hjalmars (1973), is plotted in the same figure. This curve has no local maximum and predicts an increase in the values of the critical rise with an increase in the air flow rate in contradiction with the experimental tests. It also reveals a much higher deviation from the experimental data.

A decrease in air bubble diameter from 2 mm to 1 mm leads to a drastic increase in the measured values of the critical rise from 0.35–0.8 at $\gamma = 0.045$. A maximum value of $\Delta_c = 0.85$ is then reached at $\gamma = 0.05$ and a further increase in the air flow rate gives lower values of Δ_c which decrease gradually from 0.85–0.75 at $\gamma = 0.12$. Also in this case theory is in good agreement with the measured values. The theoretical curve reaches its maximum of 0.78 at the same value of the air flow rate $\gamma = 0.05$ and drops with a further increase in γ to 0.62 at $\gamma = 0.12$. The maximum deviation of the theoretical curve from the experimental points is here approximately 18%. A curve obtained by means of the single-phase analysis disregarding friction effects shows even a greater discrepancy with the experimental data than in the case of 2 mm bubbles. The deviation from the measured values is as high as 68% at low values of air flow rates, see figure 3.

Finally theoretical curves and experimental values of the oscillation periods for the flows with two different bubble sizes are shown in figure 9. Here too, a good agreement of the theory with experiment and a considerable improvement as compared to the single-phase theory is observed.

The theory may also be compared with the observations on the 25 m pump considered by Hjalmars (1973). The observed values for this pump were in the range $\Delta_c = 0.28$–0.32 and $T = 15$–20 s. With the value $K = 4$, determined from the observations on the model pump, the theoretical results for the 25 m pump are $\Delta_c = 0.2$ and $T = 16.5$ s for $\gamma = 0.045$. The agreement is seen to be rather satisfactory, already with the K-value of the model pump, but can be improved by choosing an adjusted value $K = 8$, giving $\Delta_c = 0.25$ and $T = 18$ s, see figure 7.

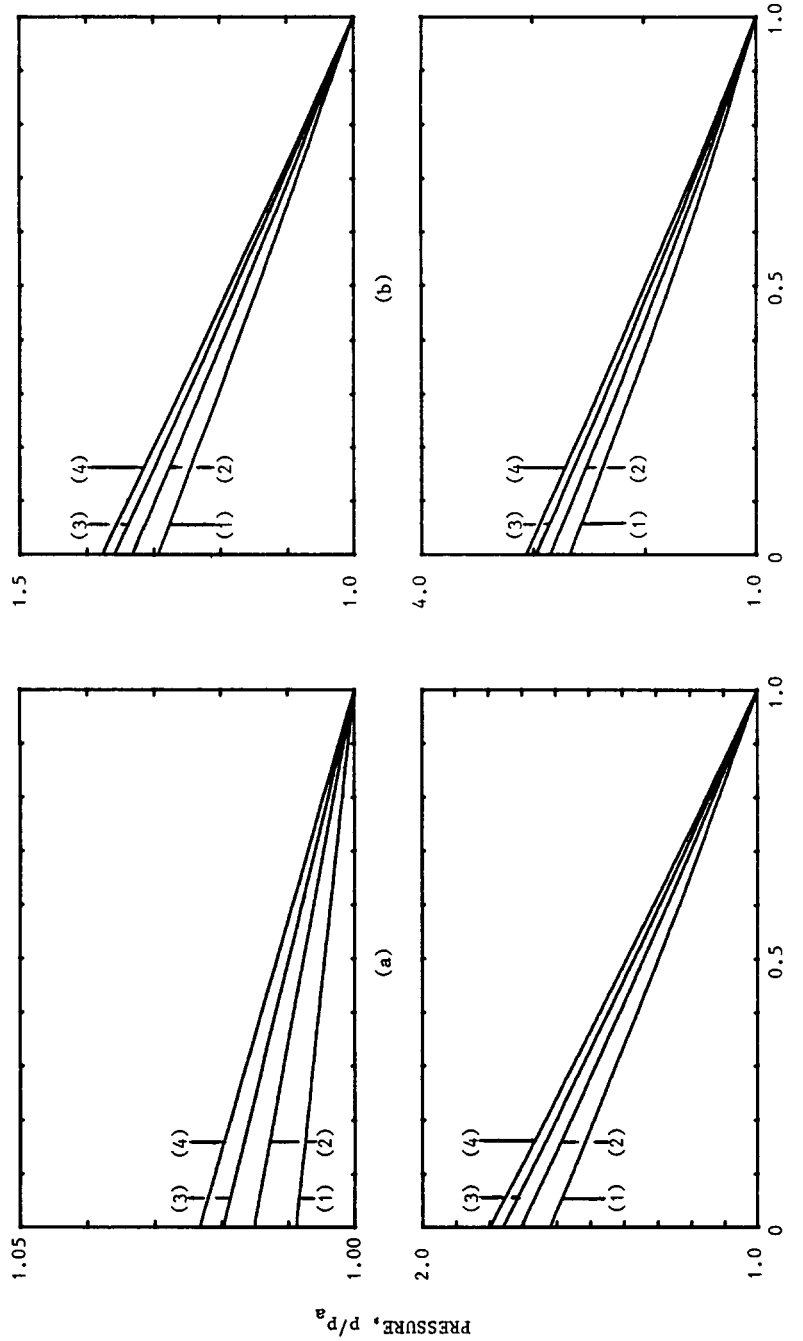

Figure 10. Variation of pressure in the pipe with height for airlift pups with various pipe lengths $r_0 = 5 \cdot 10^{-4}$ m. (a) $L = 0.49$ m, $\gamma = 0.09$, (1): $\hat{\Gamma} = 0.04$, (2): $\hat{\Gamma} = 0.06$, (3): $\hat{\Gamma} = 0.08$, (4): $\hat{\Gamma} = 0.1$; (b) $L = 5$ m, $\gamma = 0.04$, (1): $\hat{\Gamma} = 0.06$, (2): $\hat{\Gamma} = 0.08$, (3): $\hat{\Gamma} = 0.09$, (4): $\hat{\Gamma} = 0.11$; (c) $L = 10$ m, $\gamma = 0.04$, (1): $\hat{\Gamma} = 0.06$, (2): $\hat{\Gamma} = 0.08$, (3): $\hat{\Gamma} = 0.1$, (4): $\hat{\Gamma} = 0.12$; (d) $L = 25$ m $\gamma = 0.08$, (1): $\hat{\Gamma} = 0.1$, (2): $\hat{\Gamma} = 0.13$, (3): $\hat{\Gamma} = 0.15$, (4): $\hat{\Gamma} = 0.18$.

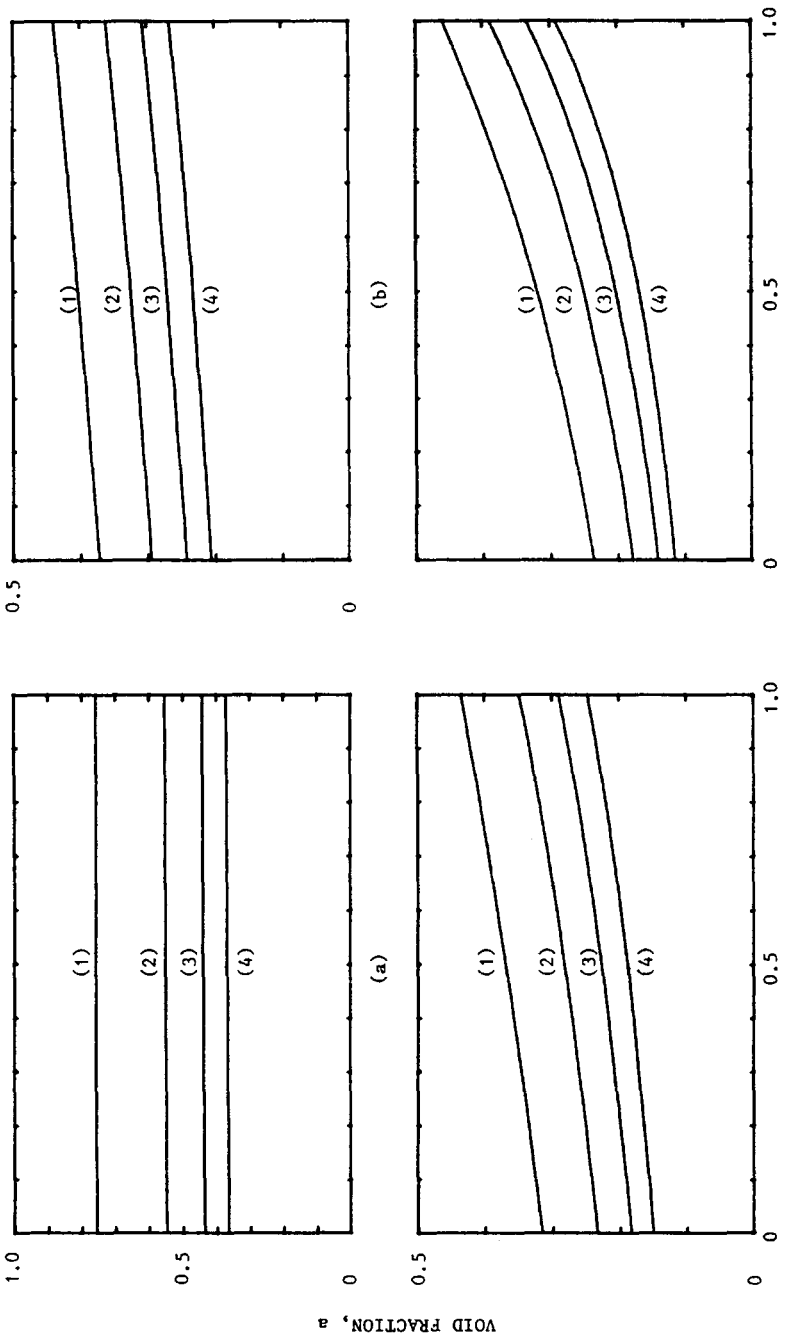

Figure 11. Variation of void fraction in the pipe with height for airlift pumps with various pipe lengths $r_0 = 5 \cdot 10^{-4}$ m. (a) $L = 0.49$ m, $\gamma = 0.09$, (1): $\hat{\Gamma} = 0.04$, (2): $\hat{\Gamma} = 0.06$, (3): $\hat{\Gamma} = 0.08$, (4): $\hat{\Gamma} = 0.1$; (b) $L = 5$ m, $\gamma = 0.04$, (1): $\hat{\Gamma} = 0.06$, (2): $\hat{\Gamma} = 0.08$, (3): $\hat{\Gamma} = 0.09$, (4): $\hat{\Gamma} = 0.11$; (c) $L = 10$ m, $\gamma = 0.04$, (1): $\hat{\Gamma} = 0.06$, (2): $\hat{\Gamma} = 0.08$, (3): $\hat{\Gamma} = 0.1$, (4): $\hat{\Gamma} = 0.12$; (d) $L = 25$ m, $\gamma = 0.08$ (1): $\hat{\Gamma} = 0.1$, (2): $\hat{\Gamma} = 0.13$, (3): $\hat{\Gamma} = 0.15$, (4): $\hat{\Gamma} = 0.18$.

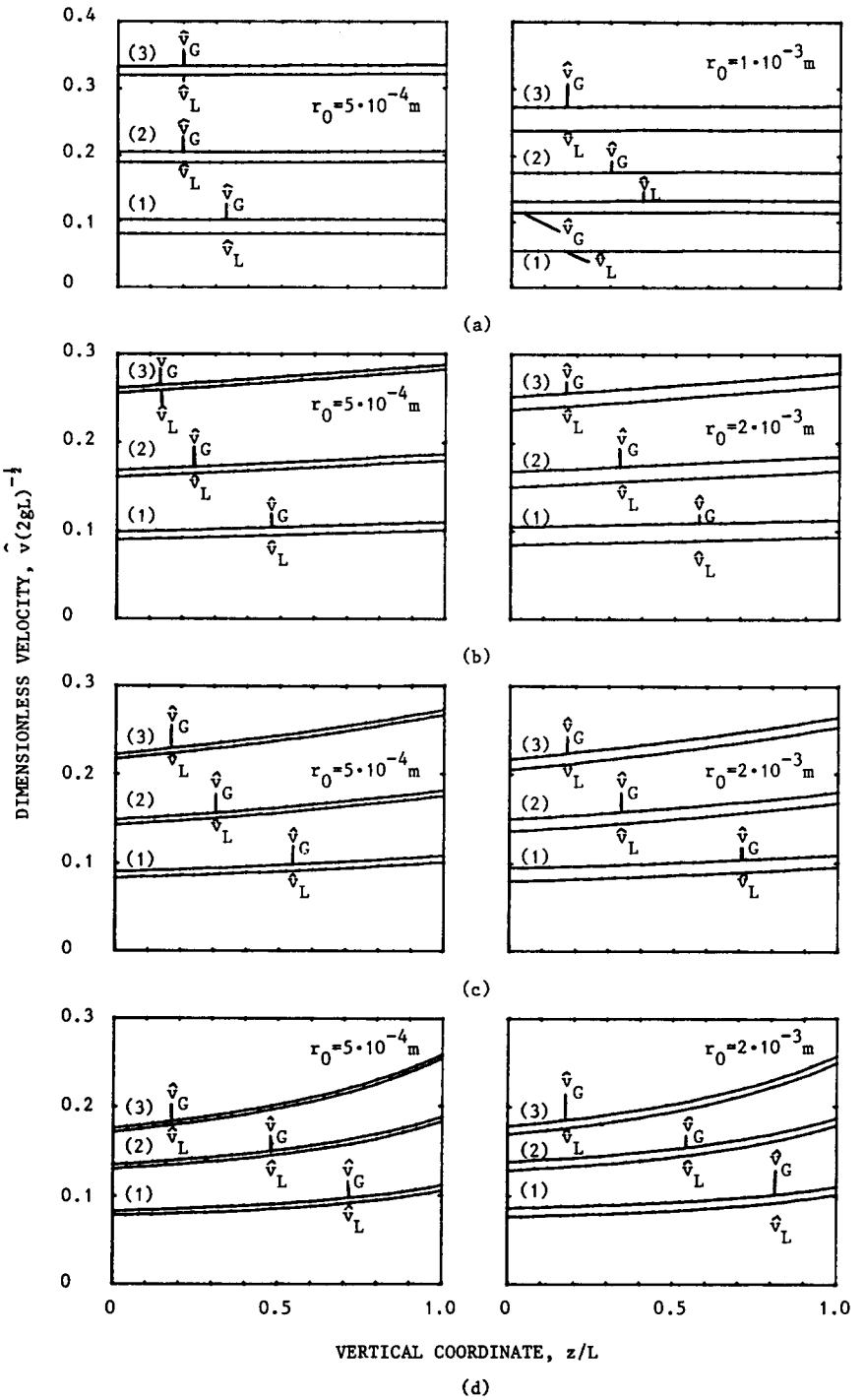

Figure 12. Variation of air and water velocities in the pipe with height for airlift pumps with various pipe lengths. (a) $L = 0.49$ m, (1): $\gamma = 0.05$, $\hat{\Gamma} = 0.03$, (2): $\gamma = 0.09$, $\hat{\Gamma} = 0.05$, (3): $\gamma = 0.13$, $\hat{\Gamma} = 0.07$, (b) $L = 5$ m, (1): $\gamma = 0.04$, $\hat{\Gamma} = 0.06$, (2): $\gamma = 0.08$, $\hat{\Gamma} = 0.08$, (3): $\gamma = 0.13$, $\hat{\Gamma} = 0.08$; (c) $L = 10$ m, (1): $\gamma = 0.04$, $\hat{\Gamma} = 0.06$, (2): $\gamma = 0.08$, $\hat{\Gamma} = 0.08$, (3): $\gamma = 0.13$, $\hat{\Gamma} = 0.11$; (d) $L = 25$ m, (1): $\gamma = 0.04$, $\hat{\Gamma} = 0.06$, (2): $\gamma = 0.08$, $\hat{\Gamma} = 0.1$, (3); $\gamma = 0.13$, $\hat{\Gamma} = 0.12$.

8. FURTHER THEORETICAL RESULTS AND DISCUSSION

Further, calculations were performed for the three pipe lengths 5 m, 10 m and 25 m in the same range of the dimensionless air and water flow rates. The value of the friction loss parameter K depends on the pump construction and should be estimated in every individual case. However, since no particular operational pump had been considered, the value of K was

taken the same as for the model airlift pump. We also neglected friction losses due to the wall friction throughout this paper. For the pipe dimensions and velocities considered here these losses are of order of magnitude 5% and less of the form type losses. Performance and stability data was obtained for each of the pumps with two different bubble diameters of 1 mm and 4 mm. For a 5 m pump the ratio of the pressure in the air injection chamber to the atmospheric pressure at the top is approximately 1.3–1.4, see figure 10(b). Figures 11 and 12 display the volumetric gas fraction and gas and water velocities in the riser as function of the vertical coordinate z. Performance data is displayed in figure 4. For a 5 m pump reduction of the bubble diameter from 4–1 mm leads to a 10% increase in the value of the rise at low

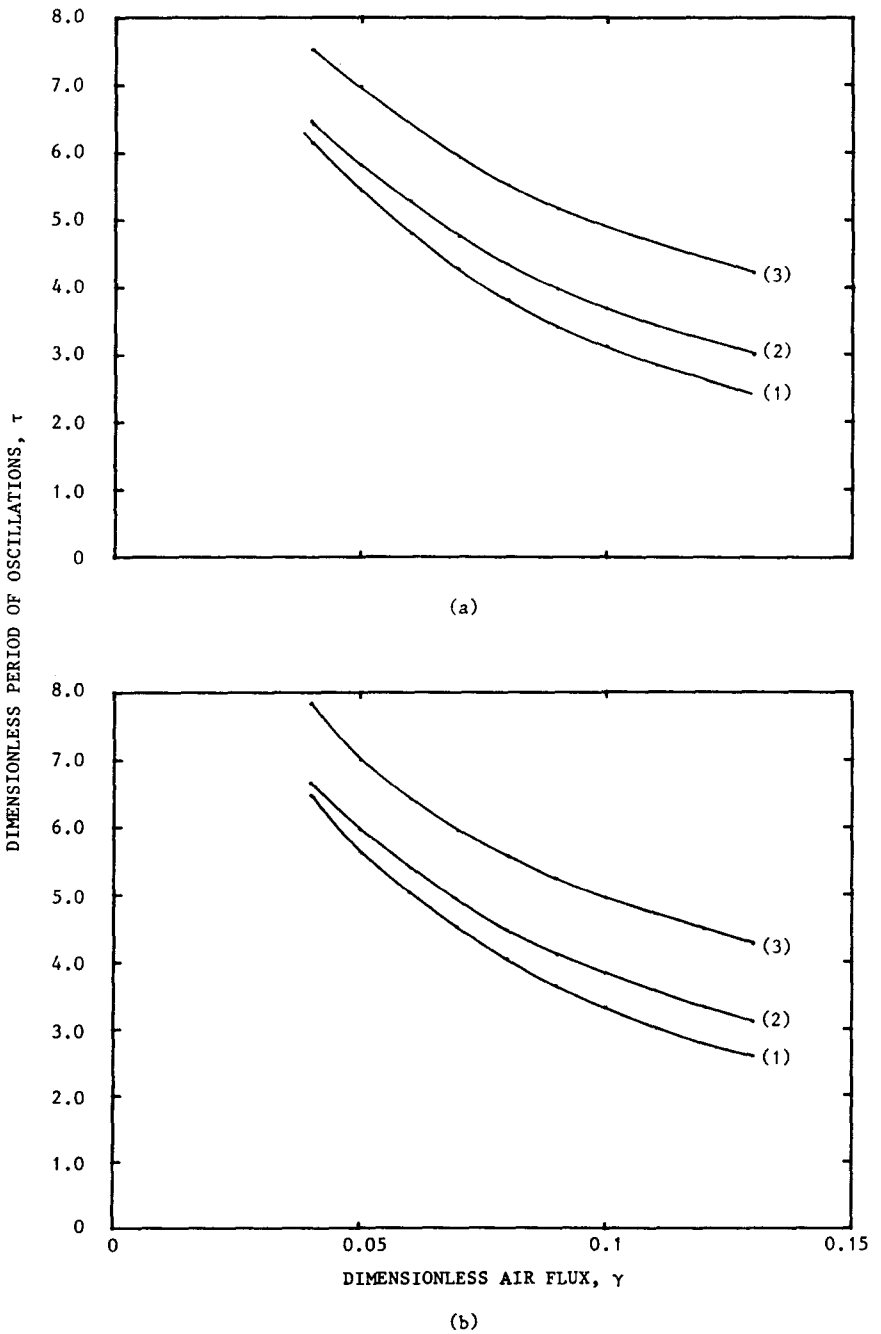

Figure 13. Theoretical values of the oscillation periods for airlift pumps with various pipe lengths. (a) $r_0 = 5 \cdot 10^{-4}$ m; (b) $r_0 = 2 \cdot 10^{-3}$ m; (1): $L = 5$ m; (2): $L = 10$ m; (3): $L = 25$ m.

values of air and water flow rates (compare the performance curves in figure 4 at $\gamma = 0.04$).

At higher flow rates, however, the difference in the slip ratio decreases and also the friction effects become dominating, which results in approximately equal values of the rise for the flows with different bubble sizes.

By increasing the pipe length to 10 m we increase the bottom to top pressure ratio to ca 1.6–1.8 see figure 10(c) which results in a greater gas expansion during the rise, see figure 11. Dimensionless phase velocities for a 10 m pump are plotted in figure 12(c). The performance curves for the two different bubble sizes (we remind that here and throughout this paper air bubble diameter is the equivalent diameter of bubbles in the air injection chamber at the bottom of the pump) are shown in figure 4(b). The performance curves are in this case steeper, because of the greater friction losses (due to an increase in the dimensional air and water flow rates). The values of the rise are also reduced because of the greater expansion losses. Reduction of the air bubble diameter from 4–1 mm gives at most a 10% increase in the values of the rise, at low air and water flow rates. At higher flow rates values of the rise become practically independent of the bubble size and thus the relative velocity.

Finally the performance of a 25 m pump is investigated. The pressure ratio in this case increases to approximately 3 see figure 10(d) which gives significant air expansion and increase in the water velocity during the rise, see figures 11(d), 12(d). Due to greater friction and expansion losses as compared to smaller pumps, lower values of the rise are obtained at the corresponding dimensionless values of the air and water flow rates, see figure 4(c). A reduction in the bubble size gives a maximum of 8% increase in the rise, this however, at low air and water flow rates, compare performance curves in figures 4(c) at $\gamma = 0.04$. With increasing air and water flow rates the curves become even less sensitive to the bubble size than for the smaller pumps.

Further the stability of the pumps with the three above-mentioned pipe lengths was investigated. Critical rise versus the dimensionless air flow rate curves for each pump and the two bubble sizes are plotted in figure 6. A drastic increase in the flow stability obtained by the air bubble size reduction for a model 0.49 m length pump is not observed for 5, 10 and 25 m length pumps. The form of the stability curves is, however, similar to that of a 0.49 m pump with a flow of 1 mm bubbles. For 5 and 10 m pumps a maximum value of the critical rise is obtained at γ approximately 0.08. A further increase in the air flow rate gives the same or even slightly lower values of the critical rise. A decrease in the bubble diameter from 4 to 1 mm leads to approximately 8 percent increase in the values of the critical rise, however again at the low values of air flow rate. At higher values of air flow rate, when the slip ratio decreases and the friction losses become more important, reduction of air bubble size and thus the relative velocity gives the same or even 2–8% lower values of the critical rise.

Acknowledgment—The author would like to acknowledge the continuing guidance and encouragement of Professor S. Hjalmars.

REFERENCES

HJALMARS, S. 1973 The origin of instability in airlift pumps. *J. Appl. Mech.* **41**, 399–404.

PEEBLES, F. N. & GARBER, H. J. 1953 Studies on the motion of gas bubbles in liquids. *Chem. Eng. Progr.* **49**, 88–97.

STENNING, A. H. & MARTIN, C. B. 1968 An analytical and experimental study of airlift pump performance. *J. Eng. Power, Trans. ASME* **90**, 106–110.

WALLIS, G. B. 1969 *One-Dimensional Two-Phase Flow.* McGraw-Hill, New York.